

# Accessible Superchiral Near-Fields Driven by Tailored Electric and Magnetic Resonances in All-Dielectric Nanostructures

Ershad Mohammadi,<sup>†,‡,✉</sup> Ahad Tavakoli,<sup>†</sup> Parisa Dehkoda,<sup>†</sup> Yasaman Jahani,<sup>‡</sup> Kosmas L. Tsakmakidis,<sup>§</sup> Andreas Tittl,<sup>‡,✉</sup> and Hatice Altug<sup>\*,‡,✉</sup>

<sup>†</sup>Department of Electrical Engineering, Amirkabir University of Technology, Tehran, Iran

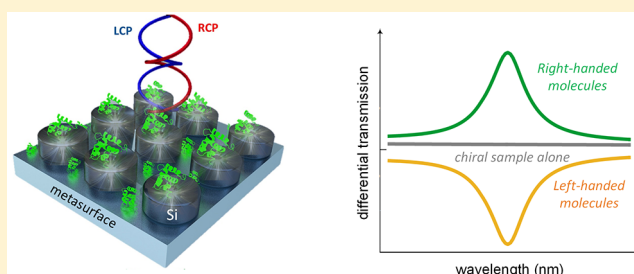
<sup>‡</sup>Bioengineering Department, École Polytechnique Fédérale de Lausanne (EPFL), 1015 Lausanne, Switzerland

<sup>§</sup>Department of Solid State Physics, National and Kapodistrian University of Athens, Panepistimioupolis, GR-157 84 Athens, Greece

## S Supporting Information

**ABSTRACT:** Detection and differentiation of enantiomers in small quantities are crucially important in many scientific fields, including biology, chemistry, and pharmacy. Chiral molecules manifest their handedness in their interaction with the chiral state of light (e.g., circularly polarized light), which is commonly leveraged in circular dichroism (CD) spectroscopy. However, compared to the linear refractive index molecular chirality is extremely weak, resulting in low detection efficiencies. Recently, it has been shown that these weak chiroptical signals can be enhanced by increasing the optical chirality of the electromagnetic fields interacting with chiral samples. Here, we show numerically and analytically that dielectric structures can provide an optimum chiral sensing platform by offering uniform superchiral near-fields. To illustrate this, we first study a simple dielectric dimer and show that circularly polarized light can induce parallel and out of phase electric and magnetic fields, which are spectrally and spatially overlapped, and therefore produce superchiral fields at the midpoint of the dimer. This behavior is in contrast to, for example, a plasmonic dimer, where the optical chirality is limited by the electric dipolar field, which is not completely out of phase with the incident magnetic field. With the insights gained from this analysis, next we develop an approach for overlapping electric and magnetic fields in a single particle, based on Kerker effect. In particular, we introduce a Kerker-inspired metasurface consisting of holey dielectric disks, which offers uniform and accessible superchiral near-fields with CD signal enhancements of nearly 24 times.

**KEYWORDS:** optical chirality, chiral sensing, circular dichroism, dielectric metasurfaces, plasmonics



Chirality is an intrinsic property of objects that are nonsuperimposable with their mirror image.<sup>1–3</sup> Many biomolecules, as well as chemically synthesized drugs, can exist in right- and left-handed forms, which are known as enantiomers.<sup>4–6</sup> The functionality of chiral molecules is often determined by their handedness, where different enantiomers show strongly contrasting behaviors in their metabolic uptake, healing potency, and toxicological side effects.<sup>7,8</sup> Therefore, efficient discrimination of chiral molecules is crucially important in many scientific fields such as structural biology, chemistry, and pharmacology.<sup>9</sup> Traditionally, circular dichroism (CD) spectroscopy has been used for enantiomeric differentiation, which exploits the interaction of chiral molecules with circularly polarized light.<sup>10–12</sup> However, for most biomolecules, the dominant CD signal is in the ultraviolet (UV) spectral range and it is typically very weak, especially when only small amounts of chiral compounds are available.<sup>13,14</sup>

In recent years, nanophotonics has provided exciting opportunities for enhancing CD signals at visible frequencies, where CD measurements are preferred due to cost and safety

aspects.<sup>15–19</sup> Nanophotonic approaches increase the chiral light–matter interaction by generating light fields with enhanced optical chirality,<sup>20,21</sup> which is defined as

$$C\{\mathbf{E}, \mathbf{H}\} = \frac{-k_0}{2c_0} \text{Im}\{\mathbf{E} \cdot \mathbf{H}^*\} \quad (1)$$

where  $k_0$  and  $c_0$  are the wavenumber and speed of light in free space, respectively, and  $\mathbf{E}$  and  $\mathbf{H}$  denote the electric and magnetic field vectors. For characterizing the interaction between a nanophotonic structure and a chiral sample, the differential absorbed (dissipated) power  $\Delta P^{\text{abs}} = P_+^{\text{abs}} - P_-^{\text{abs}}$  can be considered,<sup>19</sup> which is defined as the difference between the absorbed power values produced by illuminating the system (chiral sample and nanophotonic platform) with right-handed (RCP/+) and left-handed (LCP/−) circularly polarized light.<sup>13</sup> Taking into account the Pasteur parameter  $\kappa$  of the chiral sample,<sup>22</sup> the differential absorbed power of an optically

Received: December 22, 2018

Published: July 1, 2019

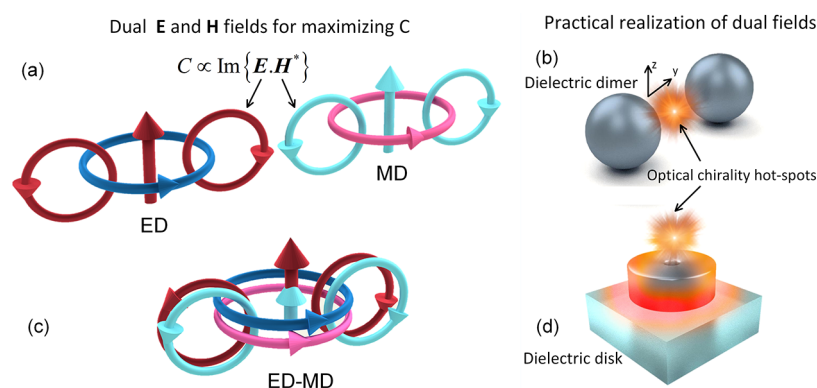


**Figure 1.** (a) Duality of electromagnetic fields in a pair of electric and magnetic dipoles (ED and MD). Both the electric (red) and magnetic (blue) field lines of the electric dipole lie parallel with the corresponding magnetic (cyan) and electric (pink) field lines of the magnetic dipole. For easier comparison, similar color tones have been chosen for electric fields (red and pink) and magnetic fields (blue and cyan). (b) Realization of the dual dipoles in panel (a) by a dielectric nanodimer composed of two high refractive index spherical nanoparticles. (c) Overlapping electric and magnetic dual dipoles in a single nanoparticle by Kerker effect. (d) Holey dielectric disk could provide overlapped dipoles shown in panel (c).

thin chiral sample interacting with the nanophotonic platform can be expressed as

$$\Delta P^{\text{abs}} = 2c_0 \text{Im}\{\kappa\} \int_{\text{sample}} (C_+ - C_-) dv \quad (2)$$

where  $C_+$  and  $C_-$  refer to the local optical chirality values provided by the nanophotonic structure for RCP and LCP illumination, respectively,<sup>20</sup> which are defined at each point inside the chiral sample (for details, see [Supporting Information](#)). The description of chiral light–matter interaction in eq 2 not only highlights the requirement of strong chiral near-fields for realizing highly sensitive chirality detection, but also emphasizes the significance of maximizing the averaged value of the chiral near-fields over the entire volume of the chiral sample.<sup>22–25</sup> As evidenced by the definition in eq 1, the optical chirality ( $C$ ) is affected by the local intensities of both the electric and the magnetic fields and an optimum structure for chiral sensing in the most general case should provide electric and magnetic field components that are (i) strong and spectrally overlapped, (ii) parallel and spatially overlapped, and finally, (iii)  $\pi/2$  out of phase.<sup>26,27</sup>

Nanophotonic structures offer a rich toolkit for controlling and manipulating electric and magnetic fields. Plasmonic nanostructures based on metallic elements have been shown to provide highly enhanced electric fields, but their magnetic modes are either weak or spectrally separated from the electric resonances.<sup>28–34</sup> As a result, obtaining superchiral and uniform fields with plasmonic structures still presents a challenge.<sup>19</sup> Recently, high refractive index dielectric nanostructures have emerged as an alternative to plasmonic resonators due to their low intrinsic loss, low heat generation, and high-quality factors,<sup>35–37</sup> enabling a wide range of applications, including sensing and surface-enhanced spectroscopy.<sup>38–41</sup> Resonators consisting of high refractive index materials have been shown to provide intense magnetic resonances while simultaneously exhibiting strong hot-spots of the electric near-field.<sup>38,42</sup> These unique resonant features of dielectric structures are promising for supporting strong and spectrally overlapped electric and magnetic fields.

In this Article, we exploit the synergistic combination of electric and magnetic resonances in dielectric nanoparticles to acquire highly chiral near-fields. To obtain parallel and spatially overlapped electric and magnetic fields, we consider a pair of

pure electric-magnetic dipoles placed next to each other, as in [Figure 1a](#). Based on the duality principle in electromagnetics,<sup>43</sup> the electric and magnetic field lines of the electric dipole (ED) lie parallel with the corresponding magnetic and electric field lines of the magnetic dipole (MD). This duality provides parallel and spatially overlapped electric and magnetic fields between two resonators and, thus, can potentially produce chiral fields. To this end, we first analyze a dielectric nanodimer and illustrate how electric and magnetic dipolar fields can be coupled out of phase under circularly polarized illumination to form intense hot-spots of optical chirality ([Figure 1b](#)). Our analytical and numerical analyses, together with a comparison to the plasmonic case, provide valuable insights into the underlying mechanism of chiral field formation and illustrate the advantages of dielectric structures over their plasmonic counterparts. Subsequently, in order to reduce structural complexity and increase the averaged value of optical chirality, we realize overlapped electric and magnetic dipoles in a single dielectric particle via the Kerker effect ([Figure 1c](#)).<sup>44–46</sup> Specifically, we utilize holey dielectric disks, as shown in [Figure 1d](#),<sup>47</sup> which enable both spectral and spatial overlap of electric and magnetic dipoles, in addition to providing accessible and highly chiral fields.<sup>42</sup> Finally, toward realizing a realistic chiral sensing platform, we propose a simple dielectric metasurface composed of Kerker-inspired high refractive index (e.g., silicon, germanium) holey disks that provide ultrachiral and uniform near-fields capable of enhancing the differential absorption by a factor of 24.

## ■ COMPARISON OF CHIRAL FIELD FORMATION IN DIELECTRIC AND PLASMONIC NANODIMERS

In order to exploit the electric and magnetic resonances of nanophotonic structures for achieving chiral fields, their associated electric and magnetic fields should satisfy the three criteria indicated above. To investigate the capability of dielectric platforms for maintaining these requirements, we consider a dielectric dimer that is composed of two spherical silicon particles of a diameter of 150 nm, separated by a distance of 10 nm along the  $y$ -axis (see [Figure 1b](#)). It should be noted that, for practical applications, without losing much of the properties, the ideal isolated spheres can be translated to dielectric disks on top of a substrate.<sup>48–50</sup> The dimer is illuminated with a right-CP light propagating in the  $z$ -

direction, in which the incident electric and magnetic fields can be expressed as

$$\begin{aligned} \mathbf{E}_{\text{inc}} &= E_0(\hat{x} - j\hat{y})\exp(-jk_0z) \\ \mathbf{H}_{\text{inc}} &= (jE_0/\eta_0)(\hat{x} - j\hat{y})\exp(-jk_0z) \end{aligned} \quad (3)$$

where  $E_0$  and  $\eta_0$  are the electric field amplitude and the free-space wave impedance, respectively. In order to highlight the key differences between plasmonic and dielectric structures for chiral field formation, we also study a plasmonic counterpart of the dielectric dimer composed of gold nanoparticles with the same dimensions.

Following the first criteria for obtaining strong chiral fields, an optimum platform for chiral sensing should provide intense  $\mathbf{E}$  and  $\mathbf{H}$  fields at the same wavelength. The dielectric dimer is well-known for offering electric/magnetic hot spots when the incident electric/magnetic field is polarized along the dimer axis.<sup>42</sup> According to eq 3, the incident CP light has electric and magnetic field components along the  $y$ -axis and, thus, excites both electric and magnetic hot-spots simultaneously. Figure 2a shows the calculated values for the electric and magnetic field enhancement at the midpoint of the dimer. It is evident that the intensity of electric and magnetic fields is enhanced within the same spectral range (gray shaded area), and consequently, the first chirality enhancement criteria mentioned above is satisfied. This behavior is in contrast to the plasmonic dimer, where the magnetic response is negligible at the electric resonance (yellow shaded area).

For the second criteria, we should ensure that the electric and magnetic field components of the hot-spots are parallel with each other. In order to give an intuitive explanation of how dielectric structures can provide this, we look into the induced electric and magnetic dipoles. An analytical study of the dielectric dimer, using the coupled electric-magnetic dipole method,<sup>38</sup> reveals that the CP light induces all components of both electric ( $p_x, p_y, p_z$ ) and magnetic dipoles ( $m_x, m_y, m_z$ ) in each spherical particle. It can be shown that the dominant coupling, which creates the hot-spots, originates from the dipole components along the dimer axis ( $p_y, m_y$ ). In Figure 2b, the dipolar fields associated with these induced dipoles are illustrated by the colored arrows which clearly shows that in the gap between the two dielectric spheres, the strong magnetic field from  $m_y$  (cyan arrows) lies parallel to the electric field from  $p_y$  (red arrows). In contrast, for the plasmonic dimer in Figure 2c, there is no dipolar magnetic field that lies parallel with that of the electric dipole (red arrows). Thus, the unique duality of fields associated with electric and magnetic dipolar resonances in dielectric structures is well-suited for enhancing the optical chirality by providing parallel electric and magnetic fields.

Next, we focus on the third criteria of  $\pi/2$  phase difference between the electric and magnetic fields. To investigate this condition, we express the electric and magnetic hot-spot phases as  $\phi_{E_h} = \phi(E_y^{\text{inc}}) - \phi_e$  and  $\phi_{H_h} = \phi(H_y^{\text{inc}}) - \phi_h$ , where  $\phi_e$  and  $\phi_h$  represent the phase retardation that the dimer imposes on the  $y$ -component of incident electric and incident magnetic fields, respectively. According to eq 3, these incident field components are already  $\pi/2$  out of phase, which results in the phase difference of  $\phi_{E_h} - \phi_{H_h} = \pi/2 - (\phi_e - \phi_h)$ , between the electric and magnetic hot-spots. We define the phase factor for the dielectric dimer as  $F_\phi = \sin(\phi_{E_h} - \phi_{H_h})$ , which is a figure of merit for the electric and magnetic hot-spots being out of

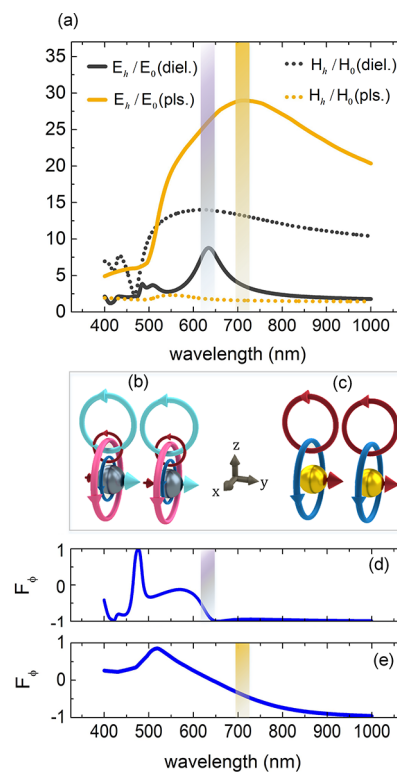


**Figure 2.** (a) Comparison between local electric and magnetic field enhancement at the midpoint of a plasmonic (gold) and a dielectric (silicon) dimer, both composed of two spherical particles of diameter 150 nm, placed 10 nm apart from each other and illuminated with CP light propagating orthogonal to the dimer axis. The gray shaded area highlights the spectral range of overlapped electric and magnetic resonances in the dielectric dimer, whereas the yellow shaded area specifies the spectral range of the electric resonance in the plasmonic dimer. (b) Sketch of the dielectric dimer aligned in the  $y$ -direction and illuminated with plane wave CP light propagating in the  $z$ -direction. Colored arrows indicate the dipolar fields associated with the induced electric and magnetic dipoles in the  $y$ -direction. (c) Sketch of the plasmonic dimer counterpart of the dielectric dimer in (b) with the same dimensions and illumination conditions. Colored arrows indicate the dipolar fields associated with the induced electric dipoles along the  $y$ -axis. The color-coding for dipolar fields is the same as in Figure 1. Red and pink denote the electric fields associated with the electric dipole and magnetic dipoles respectively, while cyan and blue represent the magnetic fields associated with the electric dipole and the magnetic dipole, respectively. (d, e) Calculated phase factors for the dielectric and plasmonic dimers, respectively.

phase. The optimal condition corresponds to  $F_\phi = \pm 1$ , which occurs, for example, when the electric and magnetic hot-spots are formed in-phase with the  $y$ -component of the incident electric and incident magnetic fields, respectively (i.e.,  $\phi_e = \phi_h = 0$ ).

In Figure 2d, the phase factor for the dielectric dimer is calculated, which shows a value close to  $-1$  (optimal condition) around the spectral overlap of the electric and magnetic resonances indicated by the gray shaded region (also in Figure 2a). For the plasmonic dimer, there is no magnetic hot-spot and thus the phase factor defined above can be reduced to  $F_\phi = \sin(\phi_{E_h} - \phi_{H_{\text{inc}}}) = \pi/2 - \phi_e$  using  $\mathbf{H}_h \approx \mathbf{H}_{\text{inc}}$  approximation. Figure 2e shows the phase factor for the plasmonic dimer around the electric resonance (indicated by the yellow shaded region), which is comparatively small (0.39)

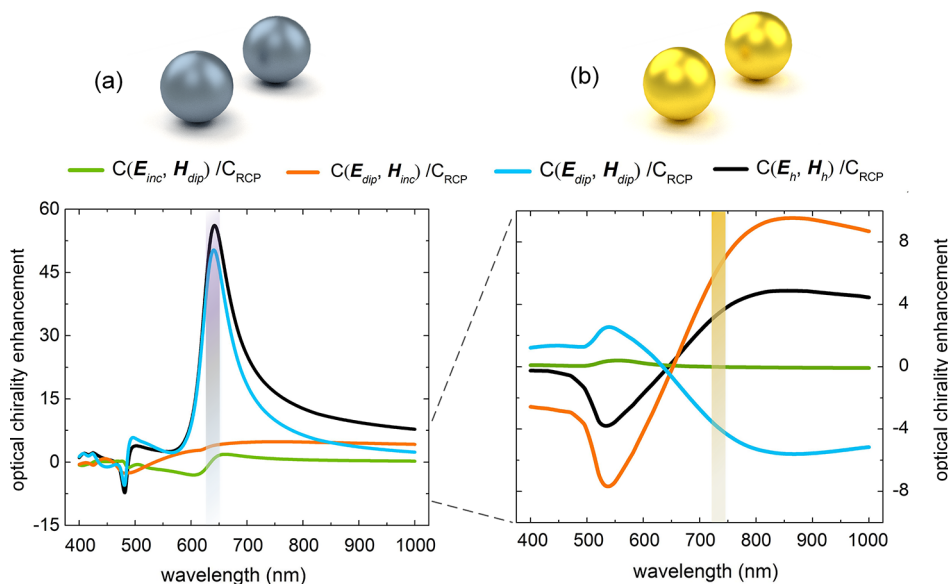


**Figure 3.** (a, b) Different contributing parts of optical chirality according to eq 4, calculated at the midpoint of the dielectric and the plasmonic nanodimers of Figure 2, respectively. Gray shaded area in (a) specifies the spectral range of overlapped electric and magnetic resonances in the dielectric dimer, while the yellow shaded area in (b) shows the spectral range of electric resonance in the plasmonic dimer.

and, therefore, significantly reduces the contribution of the electric hot-spot in enhancing the optical chirality.

Based on the aforementioned discussion, it is evident that the dielectric nanodimer is able to meet all the required conditions for the formation of chiral fields. To validate this, in Figures 3a and b, we have calculated the total optical chirality at the midpoint of the dielectric and plasmonic dimers, respectively (black curves). The dimers are the same as in Figure 2. The gray and the yellow shaded areas specify the resonance spectral ranges of the dielectric and the plasmonic dimers from Figure 2a, where we expect to observe the maximum optical chirality owing to the maximization of the dot product in eq 1. It can be seen that the total optical chirality in the dielectric dimer is stronger than in the plasmonic one, which is a direct consequence of fulfilling the three criteria studied in Figure 2. To gain further insights into the origin of optical chirality, we separate the electric and magnetic hot-spot fields ( $\mathbf{E}_h, \mathbf{H}_h$ ) into the incident and dipolar parts as  $\mathbf{E}_h = \mathbf{E}_{inc} + \mathbf{E}_{dip}$ ,  $\mathbf{H}_h = \mathbf{H}_{inc} + \mathbf{H}_{dip}$ . The normalized total optical chirality can then be decomposed into its different contributing parts as

$$\frac{C\{\mathbf{E}_h, \mathbf{H}_h\}}{C_{RCP}} = 1 - \frac{1}{2} \text{Im}\{\mathbf{E}_n^{inc} \cdot \mathbf{H}_n^{dip*}\} - \frac{1}{2} \text{Im}\{\mathbf{E}_n^{dip} \cdot \mathbf{H}_n^{inc*}\} - \frac{1}{2} \text{Im}\{\mathbf{E}_n^{dip} \cdot \mathbf{H}_n^{dip*}\} \quad (4)$$

where  $\mathbf{E}_n^{dip} = \mathbf{E}_{dip}/E_0$ ,  $\mathbf{H}_n^{dip} = \mathbf{H}_{dip}/H_0$ ,  $\mathbf{E}_n^{inc} = \mathbf{E}_{inc}/E_0$ , and  $\mathbf{H}_n^{inc} = \mathbf{H}_{inc}/H_0$  are the dipolar electric field enhancement, dipolar magnetic field enhancement, and normalized incident electric and magnetic fields, respectively (for details see Supporting Information). Equation 4 splits the total optical chirality of hot-spots into separate parts originating from the interaction of electric incident and magnetic incident ( $C\{\mathbf{E}_{inc}, \mathbf{H}_{inc}\}/C_{RCP} = 1$ ), electric incident and magnetic dipolar ( $C\{\mathbf{E}_{inc}, \mathbf{H}_{dip}\}/C_{RCP} = \text{Im}\{\mathbf{E}_n^{inc} \cdot \mathbf{H}_n^{dip*}\}/2$ ), electric dipolar and magnetic incident ( $C\{\mathbf{E}_{dip}, \mathbf{H}_{inc}\}/C_{RCP} = \text{Im}\{\mathbf{E}_n^{dip} \cdot \mathbf{H}_n^{inc*}\}/2$ ), and finally, electric dipolar and magnetic dipolar ( $C\{\mathbf{E}_{dip}, \mathbf{H}_{dip}\}/C_{RCP} = \text{Im}\{\mathbf{E}_n^{dip} \cdot \mathbf{H}_n^{dip*}\}/2$ ) fields.

Figure 3a and b present these contributing parts for the dielectric and the plasmonic dimers, respectively, which are calculated at the same point where the total optical chirality was calculated. It can be seen from Figure 3a that the dominant part of the field chirality in dielectric dimer originates from the interaction of the dipolar electric with the dipolar magnetic fields and the contribution of the two other terms is negligible. For the plasmonic dimer in Figure 3b, the dipolar magnetic field is negligible which causes the contribution of  $C\{\mathbf{E}_{inc}, \mathbf{H}_{dip}\}$  goes to zero. Taking into account the strong electric resonance of the plasmonic dimer, a significant contribution to the total optical chirality originating from  $C\{\mathbf{E}_{dip}, \mathbf{H}_{inc}\}$  and  $C\{\mathbf{E}_{dip}, \mathbf{H}_{dip}\}$  terms is expected. However, the small phase factor around the resonance wavelength reduces these values considerably. Apart from the small phase factor, these two terms show opposing magnitudes (see Figure 3b) and thus cancel out their contribution to the total optical chirality. In addition to the stronger chiral hot-spots in the dielectric dimer, the dependency of the total optical chirality on only the electric and magnetic dipolar fields (Figure 3a) introduces a simpler way for controlling the optical chirality in comparison to plasmonic dimers.<sup>24</sup>

## ■ KERKER EFFECT AND OPTIMAL CHIRAL SENSING PLATFORMS

The insights gained from studying the dielectric dimer system reveal a platform for simultaneously obtaining strong electric and magnetic fields, which are parallel and out of phase, leading to much stronger chiral fields compared to their plasmonic counterparts. One way to harness these insights in a system with reduced structural complexity is to use a single resonant dielectric disk based on the concept of the Kerker effect.<sup>44</sup> When combined into a metasurface, these dielectric disk resonators can further provide the benefit of uniform chiral near-fields owing to the periodic arrangement. According to eq 2, such uniformity is crucially important for maximizing the differential absorption signal in enhanced CD spectroscopy schemes, where the chiral sample is homogeneously distributed

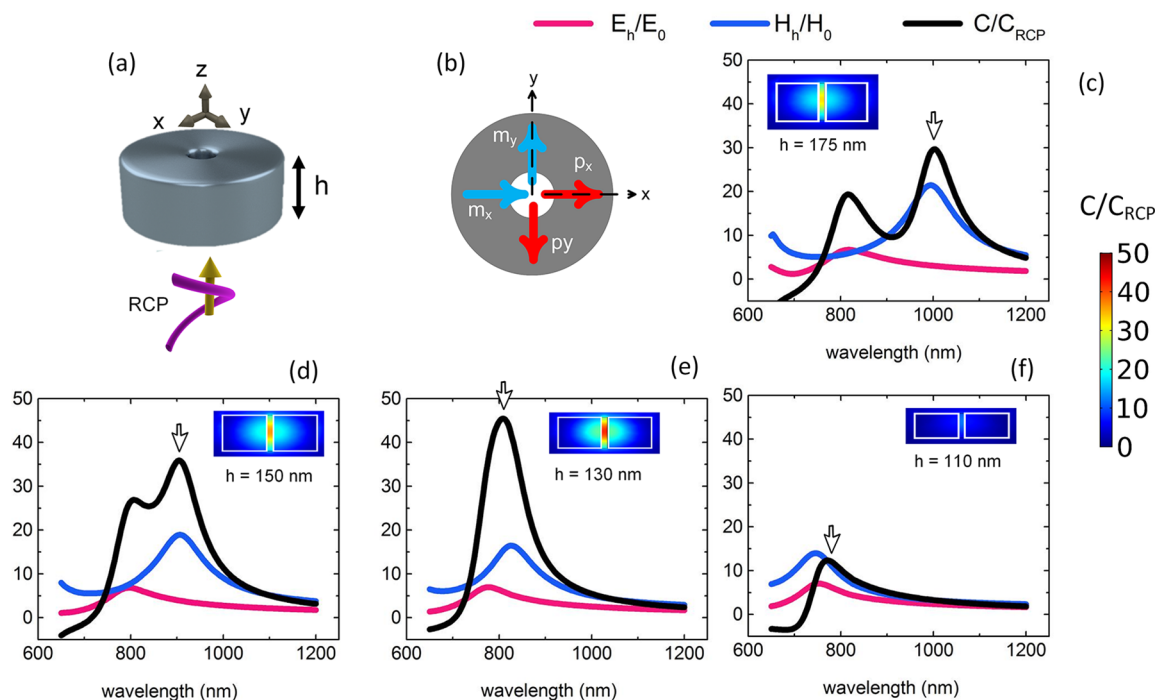


**Figure 4.** (a) Sketch of a silicon holey disk embedded in free space and illuminated with right-CP light. The diameter of the disk and its central hole are 300 and 20 nm, respectively, and  $h$  denotes the height of the particle, which is tuned for achieving overlapping electric and magnetic resonances based on the Kerker effect. (b) Cross-section of the silicon disk in the  $x$ - $y$  plane and the induced electric (red) and magnetic dipoles (blue) in  $x$ - and  $y$ -directions upon illumination by CPL light. (c–f) Electric field (pink), magnetic field (blue), and the optical chirality (black) enhancements at the center point of the holey disks for different heights. The inset in each panel shows the distribution of the maximum attainable optical chirality (marked by an arrow) for different aspect ratios.

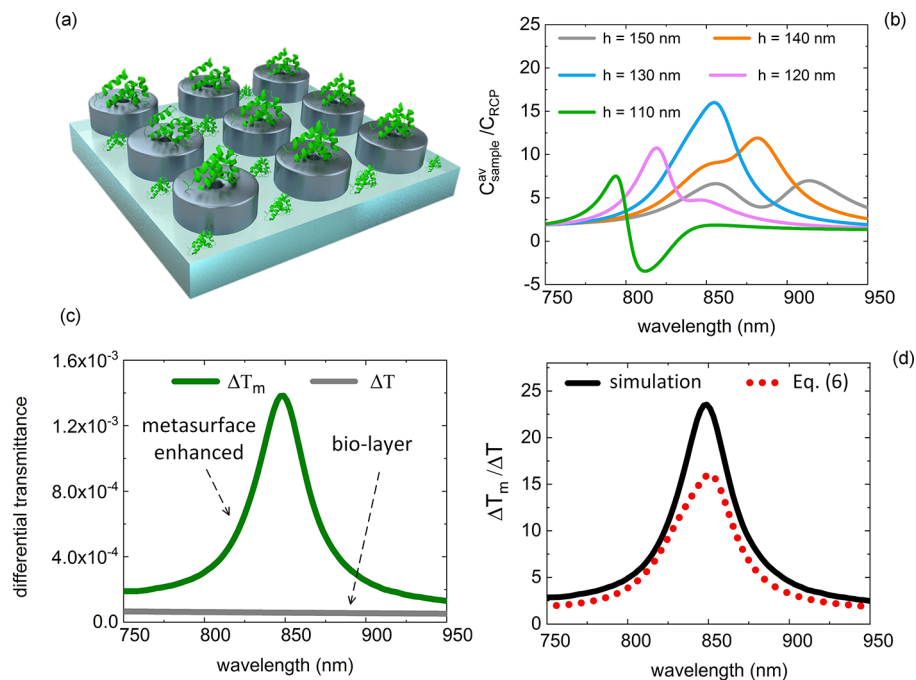


**Figure 5.** (a) Sketch of all-dielectric chiral sensing platform composed of holey silicon disks of diameter 300 nm arranged periodically with a lattice constant of 500 nm and placed on top of a glass substrate with refractive index 1.5. The central holes are 20 nm in diameter and their height is the same as the disks. The background medium on top of the glass substrate is considered as water with a refractive index of 1.33. The chiral sample is assumed to be homogeneous and described by its thickness ( $w = 20$  nm), refractive index ( $n = 1.45 - 0.01j$ ), and Pasteur parameter ( $\kappa = 0 - 0.0001j$ ). (b) Normalized averaged value of the optical chirality over the entire volume of the chiral sample for different heights of the disks when the system is illuminated with CP-light. (c) Differential transmittance of the chiral sensing platform (green), along with the differential transmittance of an individual 150 nm chiral biolayer (gray) with the same parameters, which is calculated analytically using eq 5. (d) Chiral signal enhancement in differential transmittance calculated numerically as well as analytically using eq 6.

over a nanophotonic chip. In this section, toward practical chiral sensing platforms with uniform chiral near fields, we propose a metasurface composed of a periodic arrangement of holey silicon disks. The circular silicon resonators are structurally achiral, resulting in a total CD signal that is completely free of the background chiroptical signal and only depends on the handedness of the biolayer and not on its refractive index.<sup>51</sup> To study the formation of superchiral near-fields as a consequence of the Kerker effect in dielectric disks, we consider a holey disk oriented along the  $z$ -axis, as shown in Figure 4a, which is illuminated with CP light propagating along the disk rotational axis ( $z$ ). Importantly, the holes in the disk allow direct access to the chiral hot-spots to further increase the overlap between the sample and the chiral near-fields. On the other hand, increasing the hole-size will reduce the strength of chiral near-fields. Therefore, the diameter of the hole should be chosen such that a good compromise between the accessibility and chiral hot-spot strength is achieved (see Supporting Information, section S4).

As shown in eq 3, the incident CP light has both  $x$ - and  $y$ -components of the electric and magnetic fields and can, therefore, induce the two corresponding components of the electric ( $p_x, p_y$ ) and the magnetic ( $m_x, m_y$ ) dipoles along these axes (Figure 4b). The electric and magnetic fields for the dipole pairs in each direction ( $p_x, m_x$ ) or ( $p_y, m_y$ ) were introduced in Figure 1c using duality of electromagnetic fields, but they are now realized in a single particle. In addition to the parallel and overlapped fields provided by the ( $p_x, m_x$ ) and ( $p_y, m_y$ ) dipole pairs, the incident electric field in each direction (either  $x$  or  $y$ ) has a  $\pi/2$  phase difference with the incident magnetic field in the same direction and, thus, causes  $p_x$  and  $p_y$  to oscillate  $\pi/2$  out of phase with  $m_x$  and  $m_y$ . Therefore, the disk provides two resonant and out of phase electric-magnetic dipole pairs ( $p_x, m_x$ ) and ( $p_y, m_y$ ) with spatial and spectral overlap, satisfying all requirements for generating chiral fields. In order to explore how chiral fields can be formed in the individual holey disks, we numerically simulate the response of a silicon disk of diameter 300 nm with a central symmetric hole of diameter 20 nm. In Figure 4c–f, the electric field, magnetic field, and the optical chirality enhancements are calculated at the center point of the holey disk for different disk heights varying from 175 to 110 nm. It can be seen that by changing the aspect ratio of the disk, the electric and magnetic dipole resonances of the particle (corresponding to the maxima of the  $E$  and  $H$  enhancements in each panel, that is, the pink and blue curves), approach each other so that in the case of  $h = 130$  nm, they are completely overlapped. The inset in each panel illustrates the distribution of the maximum optical chirality (marked by an arrow) associated with each disk, clearly showing that the highest amount of field chirality is observed for the Kerker case.

By recognizing the capability of silicon disks in affording strong chiral fields, we then periodically arrange holey disks with a lattice constant of 500 nm to form a dielectric metasurface, as shown in Figure 5a. The diameter of the disks and holes are the same as in Figure 4, and the structure is placed on top of a glass substrate of refractive index 1.5 to represent a structure that can be fabricated. Noting that the circularly polarized waves are eigenpolarizations of the proposed structure, the cross-polarized transmission term vanishes, which leads to the zero background chiroptical noise.<sup>51</sup> In order to evaluate this proposed metasurface for chiral sensing applications, we assume that a chiral biolayer is

attached to it, covering both the resonators and the glass substrate (Figure 5a). In accordance with practical chiral sensing schemes, the background material for the chiral molecules is considered to be water with a refractive index of 1.33. We assume that the thickness of the biolayer is 20 nm on the outer surfaces of the disk and the glass substrate and it fully covers the inside of the holes. The Pasteur parameter and the refractive index of the chiral sample are taken as  $\kappa = 0 - 0.0001j$  and  $n = 1.45 - 0.01j$ , respectively. This value of the Pasteur parameter is chosen to highlight the working principle of our metasurface-based chiral sensing scheme. Additional simulations for a Pasteur parameter with even smaller imaginary part ( $\kappa = 0 - 0.05 \times 10^{-3}j$ ) taken from chiral sensing experiments with phenylalanine molecules<sup>52</sup> are given in the Supporting Information (Figure S5). To investigate the effect of the dielectric metasurface in enhancing the CD signal, the combined system of the chiral sample on top of the nanophotonic substrate is illuminated sequentially with right- and left-circularly polarized light and the differential transmittance is measured at the output side.

Here, we consider the individual biolayer as a homogeneous chiral slab of thickness  $w$  and Pasteur parameter of  $\kappa$ . Taking into account the thin biolayer approximation ( $k_0 w \ll 1$ ), the differential transmission of the individual chiral sample can be derived as (see Supporting Information):

$$\Delta T = 4k_0 \text{Im}\{\kappa\}w \quad (5)$$

Using eq 2, it is straightforward to show that (see Supporting Information) the normalized differential transmission of the biolayer in the presence of nanophotonic platform is expressed as

$$\frac{\Delta T^m}{\Delta T} = \frac{C_{\text{sample}}^{\text{av}}}{C_{\text{RCP}}} \quad (6)$$

where  $C_{\text{RCP}}$  is the optical chirality of the incident right-CP light, and  $C_{\text{sample}}^{\text{av}}$  is the averaged optical chirality (taken over the biolayer volume), when the combined system (biolayer on top of the nanophotonic substrate), is illuminated with the same right-CP field.

Figure 5b shows the averaged optical chirality, which is taken over the biolayer volume for different heights of the disks. It is clear that for disk height of  $h = 130$  nm (i.e., the Kerker case), the maximum averaged field chirality over the chiral sample is achieved. According to eq 2, we expect that this high averaged optical chirality, which is provided by the nanophotonic substrate, enhances the differential transmission compared to the case when the biolayer is considered alone (i.e., without any nanophotonic platform). Figure 5c shows the enhanced differential transmission ( $\Delta T^m$ ) of the chiral sample on top of the metasurface for  $h = 130$  nm, which is retrieved by illuminating the system sequentially with right- and left-CP light, and then calculating the differential transmittance. We have compared the enhanced differential transmission, with the differential transmission of the chiral biolayer alone taken from eq 5. Strikingly, the nanophotonic platform has enhanced the differential transmission by a factor of 24 (see Figure 5d). In Figure 5d, the amount of enhancement is calculated analytically using eq 6, which shows a good agreement with the full-wave simulations.

## CONCLUSIONS

In summary, we have investigated the underlying mechanisms leading to the formation of highly chiral near-fields in dielectric structures. We have shown that high refractive index dielectric particles, equipped with overlapping electric and magnetic resonances, are uniquely suited for the formation of chiral fields. Specifically, in dielectric dimers, these resonant features not only enhance the local intensity of electric and magnetic fields, but also provide an ideal phase retardation ( $\pi/2$ ) between the electric and magnetic hot-spots, leading to much stronger chiral hot-spots compared to their plasmonic counterparts. Toward structures with reduced structural complexity, we exploited the Kerker effect to realize concurrent electric and magnetic dipoles in single holey disks. These disks were then arranged periodically into a metasurface to achieve uniform chiral near-fields for chiral sensing. Finally, we demonstrated that such dielectric metasurfaces can enhance the differential transmission signal of a thin chiral analyte layer by more than 1 order of magnitude, highlighting the potential of our approach for highly sensitive nanophotonics-based chiral sensing.

## ASSOCIATED CONTENT

### Supporting Information

The Supporting Information is available free of charge on the ACS Publications website at DOI: [10.1021/acsphotonics.8b01767](https://doi.org/10.1021/acsphotonics.8b01767).

S1: Differential absorbed power of a chiral sample for right- and left-circularly polarized light. S2: Decomposition of optical chirality of hot-spots into the incident and dipolar parts. S3: Nanophotonic enhancement of the differential transmittance. S4: The hole-size effect of high refractive index dielectric disks on chiral field formation. S5: Numerical simulations for additional Pasteur parameter values. (PDF)

## AUTHOR INFORMATION

### Corresponding Author

\*E-mail: [hatice.altug@epfl.ch](mailto:hatice.altug@epfl.ch).

### ORCID

Ershad Mohammadi: 0000-0001-6029-2672

Andreas Tittl: 0000-0003-3191-7164

Hatice Altug: 0000-0001-5522-1343

### Notes

The authors declare no competing financial interest.

## ACKNOWLEDGMENTS

We acknowledge the support of the European Union Horizon 2020 Framework Programme for Research and Innovation under Grant Agreement No. FETOPEN-737071 (ULTRA-CHIRAL Project) and No. 665667 (calls 2015 and 2016). Funding from the Ministry of Science, Research and Technology of the Islamic Republic of Iran is gratefully acknowledged. This project has also received funding from the Hellenic Foundation for Research and Innovation (HFRI) and the General Secretariat for Research and Technology (GSRT), under Grant Agreement No. 1819. In addition, we would like to thank Prof. Yuri Kivshar for his fruitful inputs regarding dielectric nanostructures.

## REFERENCES

- (1) Wagnière, G. H. *On Chirality and the Universal Asymmetry: Reflections on Image and Mirror Image*; John Wiley & Sons, 2008.
- (2) Gujjarro, A.; Yus, M. *The Origin of Chirality in the Molecules of Life: A Revision from Awareness to the Current Theories and Perspectives of This Unsolved Problem*; Royal Society of Chemistry, 2008.
- (3) Barron, L. D. Chirality and Life. In *Strategies of Life Detection*; Springer, 2008; pp 187–201.
- (4) Francotte, E.; Lindner, W. *Chirality in Drug Research*; Wiley-VCH: Weinheim, 2006.
- (5) Amabilino, D. B. *Chirality at the Nanoscale: Nanoparticles, Surfaces, Materials and More*; John Wiley & Sons, 2009.
- (6) Eliel, E. L.; Wilen, S. H. *Stereochemistry of Organic Compounds*; John Wiley & Sons, 2008.
- (7) Nguyen, L. A.; He, H.; Pham-Huy, C. Chiral Drugs: An Overview. *Int. J. Biomed. Sci.: IJBS* **2006**, *2*, 85.
- (8) Mitra, S.; Chopra, P. Chirality and Anaesthetic Drugs: A Review and an Update. *Indian J. Anaesth.* **2011**, *55*, 556.
- (9) H Brooks, W.; C Guida, W.; G Daniel, K. The Significance of Chirality in Drug Design and Development. *Curr. Top. Med. Chem.* **2011**, *11*, 760–770.
- (10) Fasman, G. D. *Circular Dichroism and the Conformational Analysis of Biomolecules*; Springer Science & Business Media, 2013.
- (11) Ranjbar, B.; Gill, P. Circular Dichroism Techniques: Biomolecular and Nanostructural Analyses-A Review. *Chem. Biol. Drug Des.* **2009**, *74*, 101–120.
- (12) Warnke, I.; Furche, F. Circular Dichroism: Electronic. *Wiley Interdiscip. Rev. Comput. Mol. Sci.* **2012**, *2*, 150–166.
- (13) Kelly, S. M.; Jess, T. J.; Price, N. C. How to Study Proteins by Circular Dichroism. *Biochim. Biophys. Acta, Proteins Proteomics* **2005**, *1751*, 119–139.
- (14) Sofikitis, D.; Bougas, L.; Katsoprinakis, G. E.; Spiliotis, A. K.; Loppinet, B.; Rakitzis, T. P. Evanescent-Wave and Ambient Chiral Sensing by Signal-Reversing Cavity Ringdown Polarimetry. *Nature* **2014**, *514*, 76.
- (15) Fan, Z.; Govorov, A. O. Plasmonic Circular Dichroism of Chiral Metal Nanoparticle Assemblies. *Nano Lett.* **2010**, *10*, 2580–2587.
- (16) Boriskina, S.; Zheludev, N. I. *Singular and Chiral Nanoplasmonics*; CRC Press, 2014.
- (17) Lieberman, I.; Shemer, G.; Fried, T.; Kosower, E. M.; Markovich, G. Plasmon-Resonance-Enhanced Absorption and Circular Dichroism. *Angew. Chem., Int. Ed.* **2008**, *47*, 4855–4857.
- (18) Govorov, A. O.; Gun'ko, Y. K.; Slocik, J. M.; Gérard, V. A.; Fan, Z.; Naik, R. R. Chiral Nanoparticle Assemblies: Circular Dichroism, Plasmonic Interactions, and Exciton Effects. *J. Mater. Chem.* **2011**, *21*, 16806–16818.
- (19) Schäferling, M. *Chiral Nanophotonics*. Springer Int. Publ., Switzerland, 2017.
- (20) Tang, Y.; Cohen, A. E. Optical Chirality and Its Interaction with Matter. *Phys. Rev. Lett.* **2010**, *104*, 163901.
- (21) Tang, Y.; Cohen, A. E. Enhanced Enantioselectivity in Excitation of Chiral Molecules by Superchiral Light. *Science* **2011**, *332*, 333–336.
- (22) Schäferling, M.; Yin, X.; Engheta, N.; Giessen, H. Helical Plasmonic Nanostructures as Prototypical Chiral Near-Field Sources. *ACS Photonics* **2014**, *1*, 530–537.
- (23) Tian, X.; Fang, Y.; Sun, M. Formation of Enhanced Uniform Chiral Fields in Symmetric Dimer Nanostructures. *Sci. Rep.* **2015**, *5*, 17534.
- (24) Schäferling, M.; Dregely, D.; Hentschel, M.; Giessen, H. Tailoring Enhanced Optical Chirality: Design Principles for Chiral Plasmonic Nanostructures. *Phys. Rev. X* **2012**, *2*, 31010.
- (25) Poulidakos, L. V.; Thureja, P.; Stollmann, A.; De Leo, E.; Norris, D. J. Chiral Light Design and Detection Inspired by Optical Antenna Theory. *Nano Lett.* **2018**, *18*, 4633–4640.
- (26) Schäferling, M.; Yin, X.; Giessen, H. Formation of Chiral Fields in a Symmetric Environment. *Opt. Express* **2012**, *20*, 26326–26336.

- (27) Hendry, E.; Mikhaylovskiy, R. V.; Barron, L. D.; Kadodwala, M.; Davis, T. J. Chiral Electromagnetic Fields Generated by Arrays of Nanoslits. *Nano Lett.* **2012**, *12*, 3640–3644.
- (28) Schuller, J. A.; Barnard, E. S.; Cai, W.; Jun, Y. C.; White, J. S.; Brongersma, M. L. Plasmonics for Extreme Light Concentration and Manipulation. *Nat. Mater.* **2010**, *9*, 193.
- (29) Aydin, K.; Bulu, I.; Guven, K.; Kafesaki, M.; Soukoulis, C. M.; Ozbay, E. Investigation of Magnetic Resonances for Different Split-Ring Resonator Parameters and Designs. *New J. Phys.* **2005**, *7*, 168.
- (30) Klein, M. W.; Enkrich, C.; Wegener, M.; Soukoulis, C. M.; Linden, S. Single-Slit Split-Ring Resonators at Optical Frequencies: Limits of Size Scaling. *Opt. Lett.* **2006**, *31*, 1259–1261.
- (31) Kirby, E. I.; Hamm, J. M.; Pickering, T. W.; Tsakmakidis, K. L.; Hess, O. Evanescent Gain for Slow and Stopped Light in Negative Refractive Index Heterostructures. *Phys. Rev. B: Condens. Matter Mater. Phys.* **2011**, *84*, 41103.
- (32) Mohammadi, E.; Namin, F. A.; Tsakmakidis, K. L.; Sohrabi, F.; Dehkhoda, P.; Tavakoli, A. Tunable Polarization-Sensitive Optical Nanoswitches Based on Spheroidal Core-Shell Nanoparticles. *J. Opt.* **2018**, *20*, 85004.
- (33) Tsakmakidis, K. L.; Hess, O.; Boyd, R. W.; Zhang, X. Ultraslow Waves on the Nanoscale. *Science* **2017**, *358*, eaan5196.
- (34) Ozbay, E. Plasmonics: Merging Photonics and Electronics at Nanoscale Dimensions. *Science* **2006**, *311*, 189–193.
- (35) Decker, M.; Staude, I. Resonant Dielectric Nanostructures: A Low-Loss Platform for Functional Nanophotonics. *J. Opt.* **2016**, *18*, 103001.
- (36) Albella, P.; Alcaraz de la Osa, R.; Moreno, F.; Maier, S. A. Electric and Magnetic Field Enhancement with Ultralow Heat Radiation Dielectric Nanoantennas: Considerations for Surface-Enhanced Spectroscopies. *ACS Photonics* **2014**, *1*, 524–529.
- (37) Rybin, M. V.; Koshelev, K. L.; Sadrieva, Z. F.; Samusev, K. B.; Bogdanov, A. A.; Limonov, M. F.; Kivshar, Y. S. High-Q Supercavity Modes in Subwavelength Dielectric Resonators. *Phys. Rev. Lett.* **2017**, *119*, 243901.
- (38) Albella, P.; Poyli, M. A.; Schmidt, M. K.; Maier, S. A.; Moreno, F.; Saenz, J. J.; Aizpurua, J. Low-Loss Electric and Magnetic Field-Enhanced Spectroscopy with Subwavelength Silicon Dimers. *J. Phys. Chem. C* **2013**, *117*, 13573–13584.
- (39) Caldarola, M.; Albella, P.; Cortés, E.; Rahmani, M.; Roschuk, T.; Grinblat, G.; Oulton, R. F.; Bragas, A. V.; Maier, S. A. Non-Plasmonic Nanoantennas for Surface Enhanced Spectroscopies with Ultra-Low Heat Conversion. *Nat. Commun.* **2015**, *6*, 7915.
- (40) Tittl, A.; Leitis, A.; Liu, M.; Yesilkoy, F.; Choi, D.-Y.; Neshev, D. N.; Kivshar, Y. S.; Altug, H. Imaging-Based Molecular Barcoding with Pixelated Dielectric Metasurfaces. *Science* **2018**, *360*, 1105–1109.
- (41) Krasnok, A.; Caldarola, M.; Bonod, N.; Alú, A. Spectroscopy and Biosensing with Optically Resonant Dielectric Nanostructures. *Adv. Opt. Mater.* **2018**, *6*, 1701094.
- (42) Bakker, R. M.; Permyakov, D.; Yu, Y. F.; Markovich, D.; Paniagua-Domínguez, R.; Gonzaga, L.; Samusev, A.; Kivshar, Y.; Luk'yanchuk, B.; Kuznetsov, A. I. Magnetic and Electric Hotspots with Silicon Nanodimers. *Nano Lett.* **2015**, *15*, 2137–2142.
- (43) Jackson, J. D. *Classical Electrodynamics*; Wiley, 1999.
- (44) Kerker, M.; Wang, D.-S.; Giles, C. L. Electromagnetic Scattering by Magnetic Spheres. *J. Opt. Soc. Am.* **1983**, *73*, 765–767.
- (45) Liu, W.; Kivshar, Y. S. Generalized Kerker Effects in Nanophotonics and Meta-Optics. *Opt. Express* **2018**, *26*, 13085–13105.
- (46) Yang, Z.-J.; Zhao, Q.; He, J. Boosting Magnetic Field Enhancement with Radiative Couplings of Magnetic Modes in Dielectric Nanostructures. *Opt. Express* **2017**, *25*, 15927–15937.
- (47) Baryshnikova, K. V.; Evlyukhin, A. B.; Shalin, A. S. Magnetic Hot-Spots in Hollow Silicon Cylinders. *Journal of Physics: Conference Series*; IOP Publishing, 2016; Vol. 741, p 12156.
- (48) Albella, P.; Shibanuma, T.; Maier, S. A. Switchable Directional Scattering of Electromagnetic Radiation with Subwavelength Asymmetric Silicon Dimers. *Sci. Rep.* **2016**, *5*, 18322.
- (49) Staude, I.; Miroshnichenko, A. E.; Decker, M.; Fofang, N. T.; Liu, S.; Gonzales, E.; Dominguez, J.; Luk, T. S.; Neshev, D. N.; Brener, I.; Kivshar, Y. Tailoring Directional Scattering through Magnetic and Electric Resonances in Subwavelength Silicon Nanodisks. *ACS Nano* **2013**, *7*, 7824–7832.
- (50) Shibanuma, T.; Matsui, T.; Roschuk, T.; Wojcik, J.; Mascher, P.; Albella, P.; Maier, S. A. Experimental Demonstration of Tunable Directional Scattering of Visible Light from All-Dielectric Asymmetric Dimers. *ACS Photonics* **2017**, *4*, 489–494.
- (51) Mohammadi, E.; Tsakmakidis, K. L.; Askarpour, A.; Dehkhoda, P.; Tavakoli, A.; Altug, H. Nanophotonic Platforms for Enhanced Chiral Sensing. *ACS Photonics* **2018**, *5*, 2669–2675.
- (52) García-Guirado, J.; Svedendahl, M.; Puigdollers, J.; Quidant, R. Enantiomer-Selective Molecular Sensing Using Racemic Nanoplasmonic Arrays. *Nano Lett.* **2018**, *18*, 6279–6285.